Acta Crystallographica Section F
Structural Biology and Crystallization Communications
ISSN 1744-3091

Monoclinic crystal form of *Aspergillus niger* α-amylase in complex with maltose at 1.8 Å resolution

A. Vujičić-Žagar and B. W. Dijkstra*

Laboratory of Biophysical Chemistry, University of Groningen, Nijenborgh 4, 9747AG Groningen, The Netherlands

Correspondence e-mail: b.w.dijkstra@rug.nl

Received 4 May 2006
Accepted 27 June 2006

PDB References: native *A. niger* α-amylase, 2guy, r2guysf; maltose-bound *A. niger* α-amylase, 2gvy, r2gvysf.

Aspergillus niger α-amylase catalyses the hydrolysis of α-1,4-glucosidic bonds in starch. It shows 100% sequence identity to the *A. oryzae* homologue (also called TAKA-amylase), three crystal structures of which have been published to date. Two of them belong to the orthorhombic space group $P2_12_12_1$ with one molecule per asymmetric unit and one belongs to the monoclinic space group $P2_1$ with three molecules per asymmetric unit. Here, the purification, crystallization and structure determination of *A. niger* α-amylase crystallized in the monoclinic space group $P2_1$ with two molecules per asymmetric unit in complex with maltose at 1.8 Å resolution is reported. Furthermore, a novel 1.6 Å resolution orthorhombic crystal form (space group $P2_12_12$) of the native enzyme is presented. Four maltose molecules are observed in the maltose–α-amylase complex. Three of these occupy active-site subsites −2 and −1, +1 and +2 and the hitherto unobserved subsites +4 (Asp233, Gly234) and +5 (Asp235). The fourth maltose molecule binds at the distant binding sites d1 (Tyr382) and d2 (Trp385), also previously unobserved. Furthermore, it is shown that the active-site groove permits different binding modes of sugar units at subsites +1 and +2. This flexibility of the active-site cleft close to the catalytic centre might be needed for a productive binding of substrate chains and/or release of products.

1. Introduction

Aspergillus niger α-amylase (α-1,4-glucan-4-glucanohydrolase; EC 3.2.1.1) catalyses the hydrolysis of the α-1,4-D-glucosidic linkages in starch and related oligosaccharides and polysaccharides. The enzyme has been classified as a member of glycoside hydrolase (GH) family 13 (Henrissat, 1991), which is the largest of the 109 GH families currently identified. It shows 100% sequence identity to its *A. oryzae* homologue, for which a 3.0 Å resolution crystal structure was reported as long ago as 1984 (space group $P2_1$, with unit-cell parameters a = 91.9, b = 133.3, c = 94.3 Å, β = 102.7° and three molecules per asymmetric unit; PDB code 2taa; Matsuura *et al.*, 1984). Since the *A. oryzae* enzyme was isolated from 'Takadistase Sankyo' it was named TAKA-amylase. Being the first structurally characterized GH family 13 enzyme, the TAKA-amylase structure has often been used as the representative for the entire family (Kuriki & Imanaka, 1999). Later, two $P2_12_12_1$ crystal structures were published. The first one was of the native enzyme at 2.1 Å resolution, with unit-cell parameters a = 50.9, b = 67.2, c = 132.7 Å and one molecule per asymmetric unit (PDB code 6taa; Swift *et al.*, 1991). The second was a 2.0 Å resolution structure of a complex of TAKA-amylase with the inhibitor acarbose, with unit-cell parameters a = 50.8, b = 67.1, c = 131.6 Å and one molecule per asymmetric unit (PDB code 7taa; Brzozowski & Davies, 1997). Two other crystal forms have been reported for this enzyme, but their coordinates have not been deposited in the RCSB Protein Data Bank (Berman *et al.*, 2000): a tetragonal form (space group $P4_32_12$; unit-cell parameters $a = b$ = 63.8, c = 231 Å; Akabori *et al.*, 1954; Matsuura *et al.*, 1979) and another monoclinic form (space group $P2_1$, unit-cell parameters a = 75.0, b = 104.3, c = 67.4 Å, β = 104.5°; Swift *et al.*, 1991).

The three-dimensional structures of TAKA-amylase revealed three domains: domain A (residues 1–121 and 177–380), which is the N-terminal catalytic $(\beta/\alpha)_8$-barrel domain, domain B (residues 122–

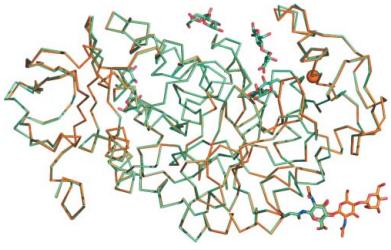

176), which is inserted between the third β-strand and the third α-helix of domain A, and domain C (residues 384–478), which is folded into an eight-stranded β-sandwich domain at the C-terminus of the enyzme. The active site is positioned at the bottom of a substrate-binding groove at the C-terminal ends of β-strands β4, β5 and β7 of the catalytic domain. Seven substrate-binding subsites (numbered from −4 to +3) were proposed for TAKA-amylase on the basis of kinetic studies performed in the early 1970s (Nitta *et al.*, 1971). Six of them were structurally characterized in a complex of TAKA-amylase with an acarbose-derived hexasaccharide (Brzozowski & Davies, 1997). The non-reducing end of the carbohydrate chain was bound at the −3 subsite, with the sugar residues extending into subsite +3 (Fig. 1*a*). Cleavage of the α-1,4-glycosidic bond in GH family 13 occurs between subsites −1 and +1 *via* a double-displacement mechanism involving a covalent glucosyl-enzyme intermediate at subsite −1 and with retention of the α-anomeric configuration of the sugar upon hydrolysis (Koshland, 1953; Uitdehaag *et al.*, 1999). Three acidic amino acids participate in the hydrolysis reaction: Glu230 acts as catalytic acid/base and Asp206 is the nucleophile, while Asp297 is involved in stabilization of the oxocarbenium ion-like transition state (Matsuura *et al.*, 1984; Uitdehaag *et al.*, 1999). We report here the purification, crystallization and structure determination of a hitherto undescribed monoclinic crystal form of the *A. niger* α-amylase in complex with maltose, the shortest chain-length substrate of this enzyme (Nitta *et al.*, 1971), at 1.8 Å resolution. Furthermore, a 1.6 Å new orthorhombic crystal form is presented ($P2_12_12$). The two molecules *A* and *B* in the asymmetric unit of the monoclinic unit cell bind four and two maltose molecules, respectively. In both proteins maltose molecules occupy subsites −1 and −2 as well as +1 and +2 in the active-site cleft. In addition, in molecule *A* two more maltose molecules are bound. One occupies the until now unobserved subsites +4 and +5 in the active-site groove. The other binds to two distant binding sites d1 and d2, also previously unobserved. These latter two binding sites are located in a loop connecting the A and C domains and could function to bind the polysaccharide chain extending from the active site. Furthermore, alternative modes of sugar binding at subsites +1 and +2 are observed when comparing the maltose–α-amylase with the acarbose–TAKA-

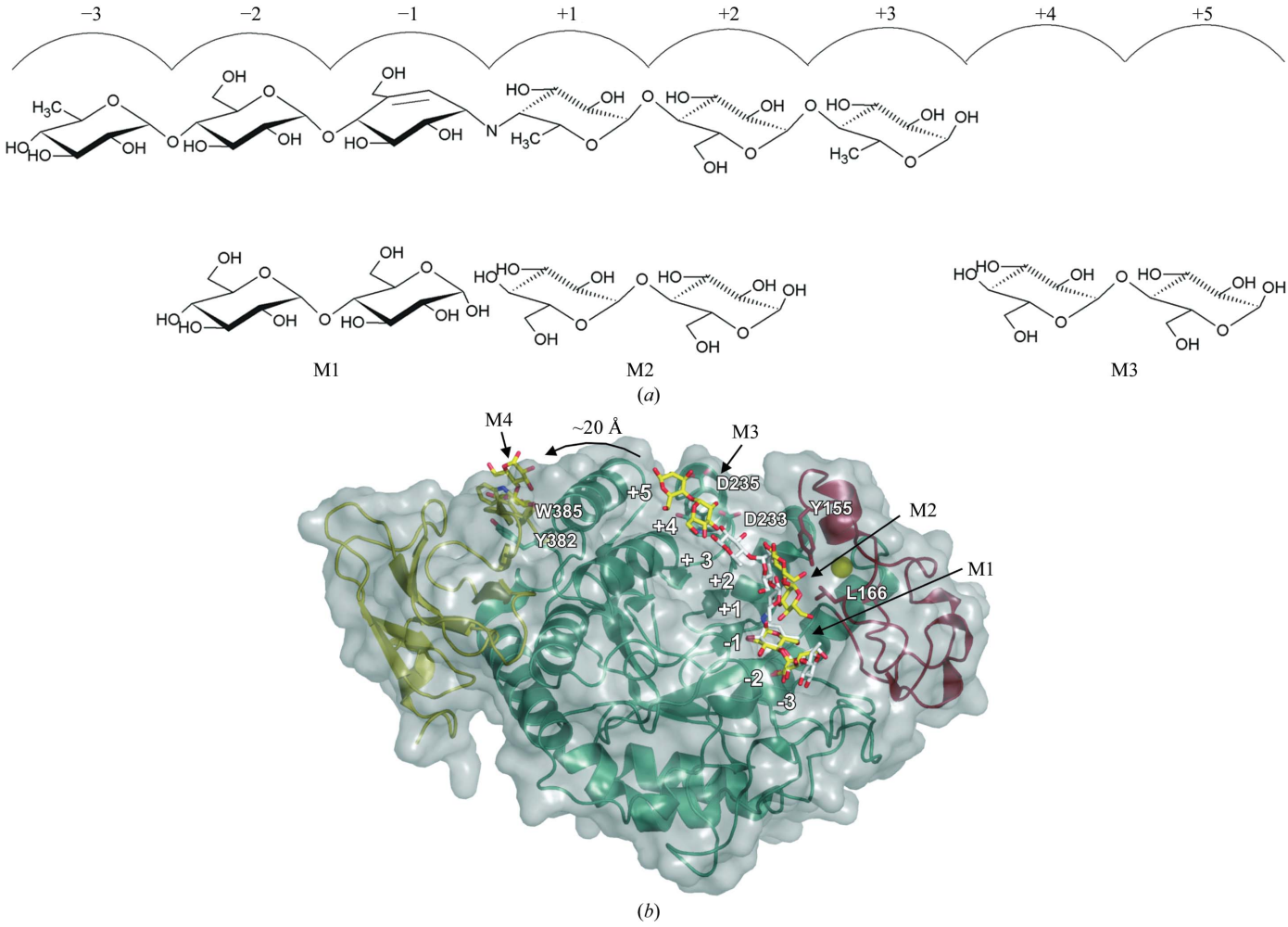

Figure 1
Maltose *versus* acarbose binding in *A. niger* α-amylase. (*a*) Schematic presentation of the acarbose-derived hexasaccharide bound in the TAKA-amylase structure (PDB code 7taa; Brzozowski & Davies, 1997) with the inhibitor acarbose bound at subsites −1 to +3. According to Brzozowski & Davies (1997), the maltosyl moiety of the hexasaccharide bound at the −3 and −2 subsites resulted from overlapping binding modes of acarbose. Beneath the hexasaccharide presentation, three maltose molecules M1, M2 and M3, which occupy subsites −2 and −1, +1 and +2, and +4 and +5, respectively, are depicted. (*b*) Molecular-surface representation of molecule *A* with bound maltose molecules M1, M2, M3 and M4 shown in yellow stick representation. The three domains A, B and C are coloured green, red and yellow, respectively. The above-mentioned hexasaccharide molecule, shown in white stick representation, is superimposed on the present structure (using the program *XtalView*; McRee, 1992). Substrate-binding subsites are numbered from −3 to +5.

Table 1
Data-collection statistics.

Values in parentheses are for the highest resolution shell.

Space group	$P2_12_12$	$P2_1$
Unit-cell parameters (Å, °)	a = 102.8, b = 63.2, c = 74.5, $\alpha = \beta = \gamma = 90$	a = 65.5, b = 101.1, c = 75.2, $\alpha = \gamma = 90$, β = 103.9
No. of molecules per ASU	1	2
Resolution range (Å)	40.00–1.59 (1.66–1.59)	50.00–1.80 (1.90–1.80)
No. of observations	453020	594910
No. of unique observations	65130	84823
Redundancy	7.0 (3.4)	7.0 (6.8)
Completeness (%)	98.6 (90.1)	96.6 (95.0)
$I/\sigma(I)$	20.5 (2.1)	17.2 (3.1)
R_{sym}† (%)	7.9 (55.6)	10.4 (57.8)

† $R_{sym} = \sum_{hkl}\sum_i |I_i(hkl) - \langle I(hkl)\rangle| / \sum_{hkl}\sum_i I(hkl)$.

Table 2
Refinement statistics.

Values in parentheses are for the highest resolution shell.

Space group	$P2_12_12$	$P2_1$
Resolution range (Å)	20.00–1.59 (1.63–1.59)	20.00–1.80 (1.85–1.80)
No. of amino-acid residues	476	476
No. of protein/solvent atoms	3688/564	7374/774
No. of NAG/MAN atoms†	38	28
No. of ligand atoms	—	137
No. of Ca^{2+} ions	1	1
R_{cryst}‡ (%)	16.4 (19.6)	16.2 (21.2)
R_{free}‡ (%)	19.6 (27.2)	21.0 (29.0)
Ramachandran statistics§ (%)		
Most favoured	97.9	98.0
Additionally allowed	2.1	2.0
R.m.s.d. from ideality		
Bond distances (Å)	0.014	0.018
Bond angles (°)	1.5	1.7
Mean B factors (Å^2)		
All protein atoms	26.3	26.9
Main-chain atoms	23.3	26.0
Side-chain atoms	25.3	27.9
Waters	39.6	33.7
NAG/MAN atoms	43.0	41.3
Ca^{2+} ion	20.4	21.3
Mean ligand¶ B factor (Å^2)		
Subsite −2	41.9	
Subsite −1	43.3	
Subsite +1	29.7	
Subsite +2	36.7	
Subsite +4	61.7	
Subsite +5	67.6	
Subsite d1	36.6	
Subsite d2	43.6	

† NAG, *N*-acetyl-D-glucosamine; MAN, mannose. ‡ $R_{cryst} = \sum |F_{calc} - F_{obs}| / \sum |F_{obs}|$, R_{free} is R_{cryst} for 5% of the unique observations not included in the refinement. § Ramachandran & Sasisekharan (1968). ¶ Bound to molecule *A* in the ASU.

amylase complexes (Brzozowski & Davies, 1997). This plasticity of the active-site groove in the proximity to the catalytic centre might be important both for the formation of the productive substrate–enzyme complex as well as for the release of the product from the +1 to +*n* subsites.

2. Materials and methods

2.1. Purification

A fermentation supernatant containing *A. niger* α-amylase was kindly provided by DSM, Delft, The Netherlands. A three-step purification protocol was established as follows. The fermentation supernatant was filtered over a 0.2 µm cutoff membrane, loaded onto a PD-10 desalting column (Amersham Biosciences, Sweden) and eluted with 10 m*M* sodium acetate buffer pH 5.5 (buffer *A*). The sample was then loaded onto a MonoQ HR 5/5 anion-exchange column and eluted with a linear gradient of 0–0.5 *M* NaCl in buffer *A*. Fractions containing the α-amylase were pooled and buffer was exchanged to 20 m*M* NaCl, 20 m*M* sodium acetate pH 5.5 using a Superdex 75 HR 10/30 gel-filtration column. Silver-stained SDS–PAGE showed that the protein was pure. The protein was concentrated to 8.8 mg ml^{-1} by ultrafiltration using a Centricon 30K.

2.2. Crystallization

Crystallization was performed using the hanging-drop vapour-diffusion technique at 296 K. Crystals were grown from two slightly different conditions. Orthorhombic crystals were grown in 3–4 weeks from drops that were obtained by mixing 1 µl protein solution (8.8 mg ml^{-1}) with 2 µl precipitant solution and that were equilibrated against 700 µl 0.1 *M* Na_2SO_4, 0.1 *M* MES buffer pH 6.5 and 30% PEG 6K (condition 1). Monoclinic crystals were obtained by mixing equal volumes (1 µl) of protein (8.8 mg ml^{-1}) and precipitant solutions over wells containing 700 µl 0.2 *M* sodium acetate, 0.1 *M* sodium cacodylate buffer pH 6.8, 30% PEG 8K (condition 2). They appeared after a week. In both cases similar rod-shaped crystals grew to dimensions of 200 × 80 × 60 µm. Crystals grown in condition 1 were soaked in cryoprotectant solution containing 0.1 *M* Na_2SO_4, 0.1 *M* MES buffer pH 6.5, 35% PEG 8K for approximately 1 min prior to flash-freezing in liquid nitrogen. Maltose-soaked crystals were prepared by transferring crystals grown in condition 2 to a solution containing 5%(*w*/*v*) maltose, 0.1 *M* Tris–HCl buffer pH 8.5, 50 m*M* NaCl, 35% PEG 8K for 24 h before cryocooling.

2.3. Data collection and processing

X-ray diffraction data from crystals grown in condition 1 were collected at beamline ID23-1, ESRF, Grenoble, France and processed using the *HKL*-2000 suite (Otwinowski & Minor, 1997). Diffraction data from maltose-soaked crystals were collected at beamline ID29, ESRF, Grenoble, France and processed using *MOSFLM* and *SCALA* from the *CCP*4 suite (Collaborative Computational Project, Number 4, 1994). The orthorhombic crystals grown under condition 1 belonged to space group $P2_12_12$, with unit-cell parameters a = 102.8, b = 63.2, c = 74.5 Å. Analysis of the Matthews coefficient (V_M = 2.3 Å^3 Da^{-1}) suggested the presence of one molecule per asymmetric unit and a solvent content of 47%. Maltose-soaked crystals grown from condition 2 crystallized in the monoclinic space group $P2_1$, with unit-cell parameters a = 65.5, b = 101.1, c = 75.2 Å, β = 103.9°. The Matthews coefficient (V_M = 2.3 Å^3 Da^{-1}) suggested the presence of two molecules per asymmetric unit (46% solvent content). Self-rotation function calculations indicated indeed the presence of a non-crystallographic twofold axis perpendicular to the twofold crystallographic *b* axis. Data-collection statistics are shown in Table 1.

2.4. Structure determination and refinement

Structures of both orthorhombic apo and monoclinic maltose-bound crystal forms were solved by molecular replacement using the program *Phaser* v.1.3 (McCoy *et al.*, 2005) with the TAKA-amylase structure (PDB code 7taa; Brzozowski & Davies, 1997) as the search model. Water, sugar molecules and ions were removed and the model was divided into two domains: the N-terminal catalytic TIM-barrel domain (residues 1–380) and the C-terminal eight-stranded anti-parallel β-sandwich domain (residues 381–478). However, this proved to be unnecessary since the $(\beta/\alpha)_8$-barrel and C-terminal domains kept the same relative orientations as in the starting model. After

rigid-body refinement of the obtained solutions, the R factors were 0.31 and 0.30 for the orthorhombic and monoclinic structures, respectively. Refinement was performed using the program *REFMAC5* (Murshudov *et al.*, 1999), setting aside 5% of the reflections to monitor refinement progress with the R_{free} factor. Water molecules, added automatically with the program *XtalView* (McRee, 1992), were checked by visual inspection. Special attention was given to the refinement of the model of the maltose-soaked crystals. In the early stages of the refinement positive electron density in an $F_{obs} - F_{calc}$ difference map contoured at 3σ revealed the presence of several bound sugar molecules, which were included in the model only at the final stages of the refinement. The quality of the models was checked using the programs *WHAT IF* (Vriend, 1990) and *MolProbity* (Davis *et al.*, 2004). Refinement statistics are shown in Table 2.

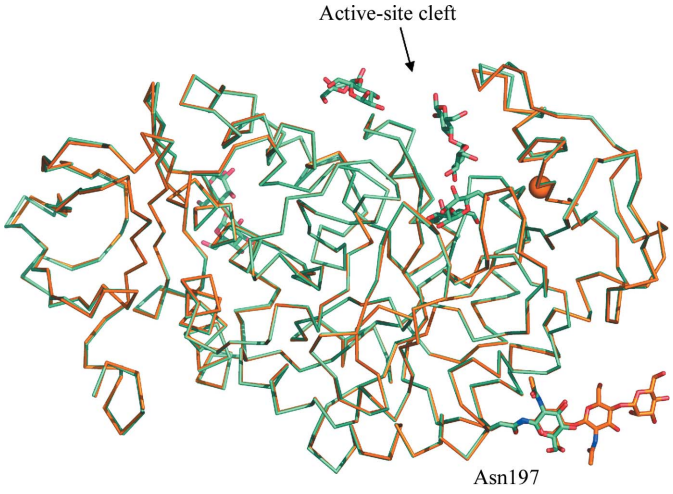

Figure 2
C^{α}-trace of superimposed $P2_1$ and $P2_12_12$ crystal structures of *A. niger* α-amylase coloured green and orange, respectively. The glycosylated side chain of Asn197 is shown in stick representation. Structure superposition was carried out using the program *XtalView* (McRee, 1992).

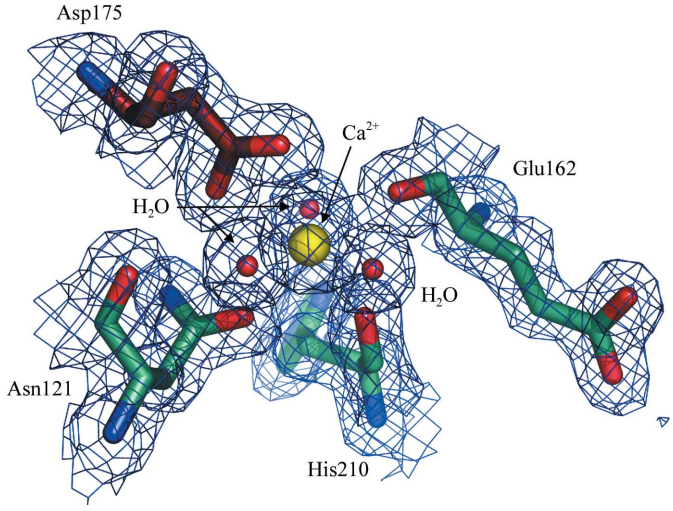

Figure 3
Electron density of the 'high-affinity' Ca^{2+}-binding site in the $P2_12_12$ *A. niger* α-amylase crystal form. The maximum-likelihood and σ_A-weighted $2F_{obs} - F_{calc}$ electron-density map contoured at the 1σ level is coloured blue. Residues Asn121, Glu162 and His210 from domain A are coloured green and Asp175 from domain B is coloured red.

3. Results and conclusions

In both the orthorhombic and monoclinic crystal structures of *A. niger* α-amylase presented here, the first 476 out of 478 amino-acid residues could be built. Furthermore, the electron density attached to Asn197 in the orthorhombic structure enabled us to model three sugar units (two *N*-acetyl-D-glucosamine residues and one mannose), while one *N*-acetyl-D-glucosamine unit could be built in the monoclinic structure (Fig. 2). One Ca^{2+} ion is bound to the 'high-affinity' binding site

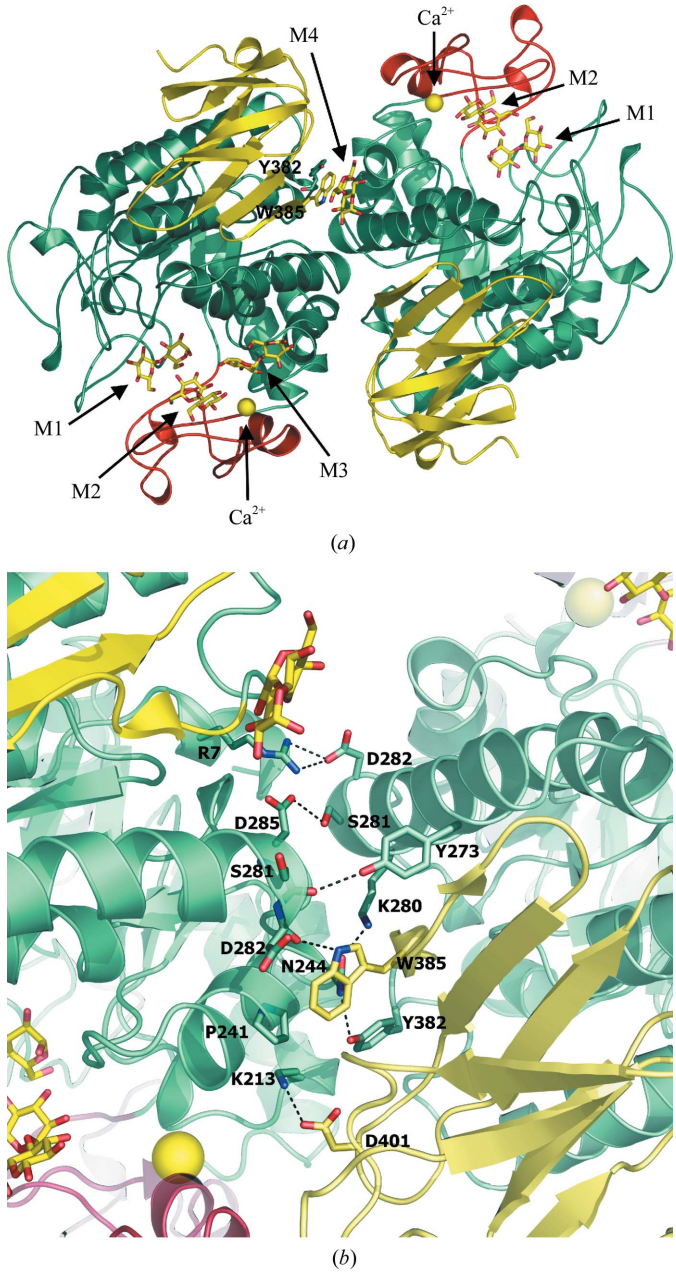

Figure 4
Dimer formation in the $P2_1$ unit cell. (*a*) Ribbon representation of molecules *A* (left) and *B* (right) forming the dimer. Domains A, B and C are colored green, red and yellow, respectively. The Ca^{2+} ion is depicted as a yellow sphere. Maltose molecules M1, M2, M3 and M4 are coloured yellow and shown in stick representation. Residues Tyr382 and Trp385 in molecule *A* make aromatic stacking interactions with maltose M4. (*b*) Dimer interface. Residues involved in forming the dimer are shown in stick representation. Hydrogen-bonding and salt-bridge interactions are shown as dashed lines and coloured black.

in both crystal forms with the same octahedral coordination as described previously by Boel *et al.* (1990) (Fig. 3).

3.1. Differences in crystal packing between the monoclinic $P2_1$ and the orthorhombic $P2_12_12$ crystal forms

The orthorhombic and monoclinic crystal structures of *A. niger* α-amylase superimpose with an r.m.s. difference of 0.22 Å for all C^{α} atoms, indicating almost identical conformations (Fig. 2). The unit-cell parameters in these two crystal forms are related (see Table 1), with the difference that the $P2_1$ *b* axis becomes the *a* axis in the $P2_12_12$ unit cell and that the β angle in the monoclinic unit cell is $\sim$104°. The crystal packing of the enzyme in these two space groups is similar, with one noteworthy difference. The two molecules (*A* and *B*) in the asymmetric unit of the $P2_1$ unit cell are related by an improper non-crystallographic twofold symmetry axis parallel to the crystallographic *a* axis, forming an artefactual dimer (Fig. 4*a*). The two molecules have extensive interactions, burying approximately 1100 $Å^2$ of surface area (calculations performed using *CNS*; Brünger *et al.*, 1998), compared with an average of 530 $\pm$ 160 $Å^2$ buried in the interface between the molecules related by space-group symmetry. Moreover, the contacts between the two dimer molecules consist of polar, hydrophobic and salt-bridge interactions, while solely polar interactions keep together the other molecules in the crystal. The residues involved in formation of the dimer interface are shown in Fig. 4(*b*). In contrast, the dimer-like packing is absent in the orthorhombic unit cell, where a twofold screw rotation relates the molecules (Fig. 5*b*). The interactions between these latter two molecules are not different from the other intermolecular contacts present in the orthorhombic crystal; the contacts are of a polar nature and bury 690 $Å^2$ of surface area compared with an average of 660 $\pm$ 95 $Å^2$. We believe that this dimer formation of the *A. niger* α-amylase is a result of crystal packing. This is evident from the comparison of crystal packing in the related monoclinic and orthorhombic unit cells presented here. In the $P2_1$ unit cell the improper NCS twofold symmetry axis has a translational component along the (*a*) axis shorter than half a unit-cell length (0.27) that keeps the two molecules closer together. On the other hand, a full crystallographic half cell-length translation along the corresponding (*b*) axis in the $P2_12_12$ unit cell sets the two molecules apart (see Fig. 5). That the dimer formation in the monoclinic unit cell has no biological relevance is furthermore in agreement with dynamic light-scattering (DLS) experiments on a concentrated protein sample (8.8 mg ml^{-1} in 20 m*M* sodium acetate buffer pH 5.5, 20 m*M* NaCl, data not shown),

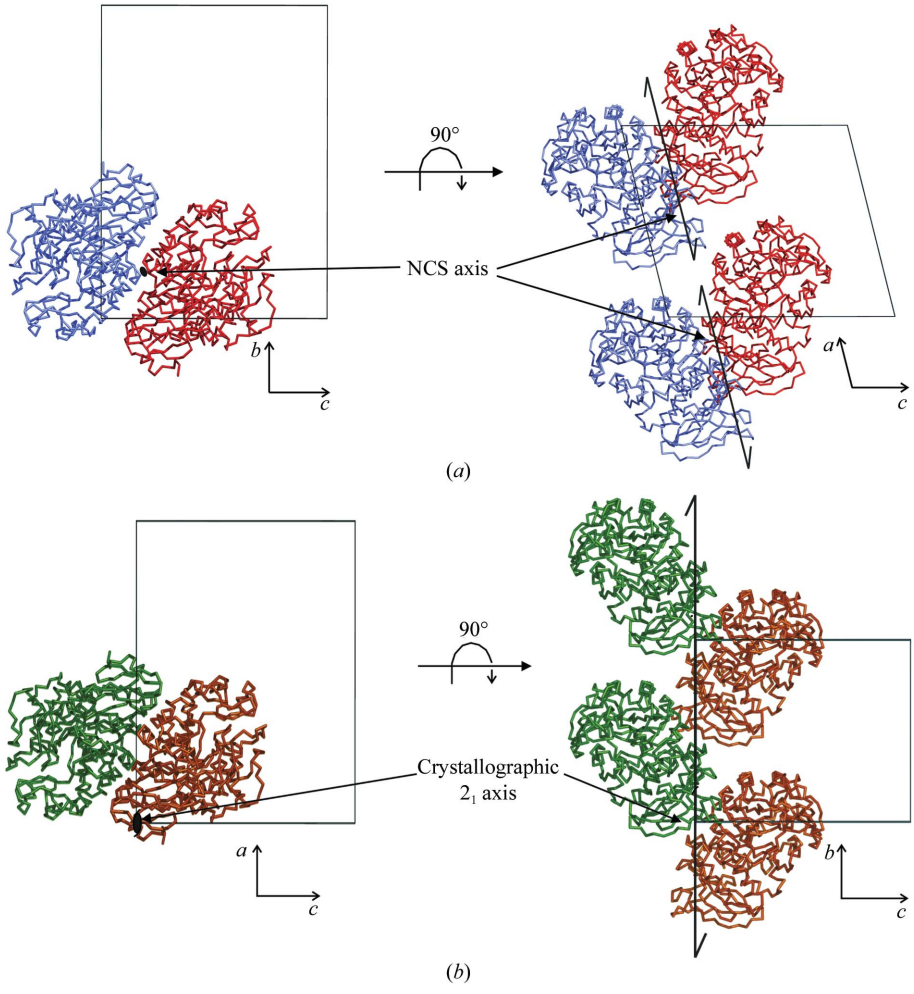

Figure 5
Crystal packing in the $P2_1$ and $P2_12_12$ unit cells. (*a*) Dimer packing in the $P2_1$ unit cell. The position of the improper non-crystallographic twofold symmetry axis perpendicular to the crystallographic twofold screw *b* axis is shown in the *bc* and *ac* planes on the left and right, respectively. (*b*) Crystal packing in the $P2_12_12$ unit cell. The $P2_1$ *b* axis becomes the *a* axis in the $P2_12_12$ unit cell (see Table 1). Dimer packing as seen in the monoclinic unit cell is absent in the $P2_12_12$ cell owing to a twofold screw axis along *b* which imposes a full half cell-length translation.

which indicated a molecular mass of 48 kDa for the enzyme in solution compared with the theoretical mass of 52 kDa for a non-glycosylated monomeric enzyme.

3.2. Monoclinic maltose-bound α-amylase crystal structure

The active sites of both molecules *A* and *B* in the asymmetric unit of the monoclinic unit cell each show clear electron density for two maltose molecules bound at subsites −2 and −1 (M1) and +1 and +2 (M2). Two additional maltose molecules (M3 and M4) are bound only to molecule *A*. Molecule M3 occupies the previously unobserved subsites +4 and +5 in the active-site groove, while molecule M4 is bound at distant binding sites named d1 and d2 located in a loop connecting the catalytic A and the C domain (Fig. 4*a*). The latter two sites are not available in molecule *B* owing to crystal contacts (Fig. 4*b*).

3.2.1. Maltose binding at the −1 and −2 subsites. The maltose molecule bound at subsites −1 and −2 resembles the binding mode of valienamine (subsite −1) and 4-amino-4,6-dideoxy-α-D-glucose (subsite −2) in the acarbose–TAKA-amylase complex (Brzozowski & Davies, 1997). They superimpose with an r.m.s. difference of 0.28 Å for the sugar-ring atoms (Fig. 1*b*). The major difference between the glucose residue of the maltose and the valienamine unit of acarbose at subsite −1 is the conformation of the pyranose ring. In the acarbose–TAKA-amylase complex the unsaturated valienamine ring is bound in a $^2H_3$ half-chair-like conformation with the C4–C5–C7–C1 atoms defining the plane that is believed to resemble the oxo-carbenium ion-like transition state (Brzozowski & Davies, 1997). The corresponding glucose unit in the maltose-α-amylase complex has the relaxed $^4C_1$ chair conformation which a sugar residue at this subsite would assume after hydrolysis of the glucosyl-enzyme intermediate, before leaving the active-site cleft.

3.2.2. Maltose binding at the +1 and +2 subsites. The M2 maltose molecule is shifted approximately 2.5 Å towards the Tyr155 and Leu166 residues at the 'opposite side' of the substrate-binding groove compared with the bound acarbose-derived hexasaccharide in the acarbose–TAKA-amylase complex (Fig. 1*b*). The +1 glucosyl unit makes van der Waals interactions with Leu166, whereas the pyranose ring of the +2 sugar is involved in hydrophobic stacking interactions with Tyr155. Hence, the active-site groove permits alternative sugar-binding modes at these subsites. This plasticity of the active-site groove close to the catalytic centre might be needed in order to allow conformational changes of the carbohydrate chain until a productive substrate–enzyme complex is formed. Moreover, the plasticity of this particular part of the active-site cleft might be important for the release of the polysaccharide chain bound at subsites +1 to +*n* after cleavage of the scissile glycosidic bond and formation of the glucosyl-enzyme intermediate has taken place. Indeed, if binding of the acarbose-derived hexasaccharide represents the productive way of binding of the carbohydrate chain, then binding of the maltose molecule M2 may show the binding mode of sugar units after the α-1,4-glucosidic bond of the substrate has been cleaved and before the first product has been released from the active site.

3.2.3. Binding of maltose molecules M3 and M4 to molecule *A*. Maltose molecule M3, which occupies the newly identified subsites +4 and +5, makes long hydrogen-bonding interactions with the side chain of Asp233 and the backbone N atom of Gly234 in subsite +4 and with the side chain of Asp235 in subsite +5 (Fig. 1*b*). This M3 maltose molecule is less tightly bound to the enzyme than the other bound maltose molecules, as reflected by the significantly higher *B* factors of M3 compared with those of the M1, M2 and M4 molecules (see Table 2). The M4 maltose molecule makes hydrophobic stacking interactions with Tyr382 (d1 binding site) and Trp385 (d2 binding site) located in the loop connecting the last α-helix of the TIM barrel and the first β-strand of the C domain (Fig. 4*a*). These distant binding sites are approximately 20 Å or four glucosyl units away from the active-site +5 subsite and could be involved in binding of a long carbohydrate chain extending from the active site (Fig. 1*b*).

In conclusion, two new high-resolution crystal forms of *A. niger* α-amylase with related unit-cell parameters are reported. Additionally, a monoclinic crystal form of *A. niger* α-amylase in complex with maltose at 1.8 Å resolution revealed four novel substrate-binding sites (+4, +5, d1 and d2) that might have a physiological role in binding polysaccharide chains. Furthermore, it has been shown that the active-site groove permits different binding modes of sugar units at subsites +1 and +2. This plasticity of the active-site cleft close to the catalytic centre might be needed for the formation of a productive substrate–enzyme complex and/or for releasing the products from the +1 to +*n* subsites.

The authors thank the staff at beamlines ID23-1 and ID29 at the ESRF, Grenoble, France for their assistance during data collection and DSM for providing the protein sample. The investigations were supported by Senter IOP, The Netherlands (IGE01021). All figures were generated using the program *PyMOL* v.0.98 (DeLano, 2002).

References

Akabori, S., Ikenaka, T. & Hagihara, B. (1954). *J. Biochem.* **41**, 577–582.
Berman, H. M., Westbrook, J., Feng, Z., Gilliland, G., Bhat, T. H., Wiessig, H., Shindyalov, I. N. & Bourne, P. E. (2000). *Nucleic Acids Res.* **28**, 235–242.
Boel, E., Brady, L., Brzozowski, A. M., Derewenda, Z., Dodson, G. G., Jensen, V. J., Petersen, S. B., Swift, H., Thim, L. & Woldike, H. F. (1990). *Biochemistry*, **29**, 6244–6249.
Brünger, A. T., Adams, P. D., Clore, G. M., DeLano, W. L., Gros, P., Grosse-Kunstleve, R. W., Jiang, J.-S., Kuszewski, J., Nilges, M., Pannu, N. S., Read, R. J., Rice, L. M., Simonson, T. & Warren, G. L. (1998). *Acta Cryst.* D**54**, 905–921.
Brzozowski, A. M. & Davies, G. J. (1997). *Biochemistry*, **36**, 10837–10845.
Collaborative Computational Project, Number 4 (1994). *Acta Cryst.* D**50**, 760–763.
Davis, I. W., Murray, L. W., Richardson, J. S. & Richardson, D. C. (2004). *Nucleic Acids Res.* **32**, W615–W619.
DeLano, W. L. (2002). *The PyMOL Molecular Visualization System.* http://www.pymol.org.
Henrissat, B. (1991). *Biochem. J.* **280**, 309–316.
Koshland, D. E. (1953). *Biol. Rev.* **28**, 416–336.
Kuriki, T. & Imanaka, T. (1999). *J. Biosci. Bioeng.* **87**, 557–565.
McCoy, A. J., Grosse-Kunstleve, R. W., Storoni, L. C. & Read, R. J. (2005). *Acta Cryst.* D**61**, 458–464.
McRee, D. E. (1992). *J. Mol. Graph.* **10**, 44–46.
Matsuura, Y., Kusunoki, M., Date, W., Harada, S., Bando, S., Tanaka, N. & Kakudo, M. (1979). *J. Biochem.* **86**, 1773–1783.
Matsuura, Y., Kusunoki, M., Harada, W. & Kakudo, M. (1984). *J. Biochem.* **95**, 697–702.
Murshudov, G. N., Vagin, A. A., Lebedev, A., Wilson, K. S. & Dodson, E. J. (1999). *Acta Cryst.* D**55**, 247–255.
Nitta, Y., Mizushima, M., Hiromi, K. & Ono, S. (1971). *J. Biochem.* **69**, 567–576.
Otwinowski, Z. & Minor, W. (1997). *Methods Enzymol.* **276**, 307–326.
Ramachandran, G. N. & Sasisekharan, V. (1968). *Adv. Protein Chem.* **23**, 283–438.
Swift, H. J., Brady, L., Derewenda, Z. S., Dodson, E. J., Dodson, G. G., Turkenburg, J. P. & Wilkinson, A. J. (1991). *Acta Cryst.* B**47**, 535–544.
Uitdehaag, J. C. M., Mosi, R., Kalk, K. H., van der Veen, B. V., Dijkhuizen, L., Withers, S. G. & Dijkstra, B. W. (1999). *Nature Struct. Biol.* **6**, 432–436.
Vriend, G. (1990). *J. Mol. Graph.* **8**, 52–56.